Modelling dynamic loadings of a Tidal Stream Turbine in combined wave-current-turbulence environment

Qian Li[a,*], Vengatesan Venugopal[a], Nigel Barltrop[b]

[a] *Institute for Energy Systems, School of Engineering, The University of Edinburgh, Kings Buildings, Edinburgh, EH9 3DW, United Kingdom*
[b] *Naval Architecture, Ocean and Marine Engineering, University of Strathclyde, 100 Montrose Street Glasgow, G4 0LZ*

Abstract

The understanding of hydrodynamic loadings on a Tidal Stream Turbine (TST) is important to its design, deployment and operation. An assessment involving combined wave-current-turbulence effects is essential for the prediction of the loadings and turbine performance. TSTs are often located in regions of localized high current, so the incident waves will be modified as they travel onto that higher current. This paper proposes a methodology which is capable of generating the combined wave-current effects with the integration of a model of the incident turbulence. The algorithm and methodology presented in this paper are implemented in the OpenFAST software. The modified numerical model has been validated by comparing its outputs to the scale model tests conducted in Edinburgh University's FloWave wave-current facility. The impact of combined waves, currents, and turbulence intensity on power production of a TST has been quantitatively investigated. The results show that the wave-current interaction effects are significant, in particular when waves travel in opposite direction to currents; in which case the loads were underestimated by 40.3% in comparison to excluding the wave-current interaction effects. Furthermore, the ambient turbulent flow is observed to affect the loadings and the performance of the TST, and the output suggests a discrepancy around 45.6% between different turbulence intensity levels.

Keywords: Tidal stream turbine, wave-current interaction, turbulent model, turbulence intensity, turbine performance, loadings

*Corresponding author
Email address: `qian.li-2@ed.ac.uk` (Qian Li)

This is a peer reviewed, accepted author manuscript of the following article: Li, Q., Venugopal, V., & Barltrop, N. (2022). Modelling dynamic loadings of a tidal stream turbine in combined wave-current-turbulence environment. Sustainable Energy Technologies and Assessments, 50, [101795]. https://doi.org/10.1016/j.seta.2021.101795

1. Introduction

Tidal energy possesses great potential as a sustainable and predictable energy resource. In recent decades, many tidal energy technology concepts have been proposed, built and tested either in the laboratory or in the field [1]. Among them, the horizontal axis tidal turbines (HATTs) are currently the dominant device type [1]. Although, these types of technologies are proven to work well, there is still space for research to improve their performance which will reduce the various costs involved. The hydrodynamic loadings on a TST at a specific site depend on the combination of mean current flow, orbital wave and turbulence. The inflow representing the true environment is essential in the prediction of the loading, power and thrust characteristic of the TST, especially in the combined wave-current environment in either following or opposing wave condition [2, 3, 4, 5, 6]. In the presence of waves, significant cyclic variations which occurred at the frequency of the waves were observed in the power and thrust outputs, even though the mean coefficients of power and thrust in the unsteady flow conditions have not been modulated by waves and remain similar to the steady flow values [7]. In terms of wave-current interactions, the combined irregular wave and current loads on a fully instrumented 1:15 scale model were investigated by Draycott *et al.*[8] in both waves following and opposing the currents. This study revealed that, for the waves opposing the currents, the fluctuating loads were significantly higher than the corresponding loads measured for the following and non-current cases which indicates that more fatigue damage will be accumulated, although the mean values of the load are unchanged.

The other challenge, in addition to wave-current interactions, is the evaluation of how ambient turbulence affects the performance of the TST. The instantaneous power generated by a TST has been found to be highly influenced by the turbulent features of the flow [9]. It is also known that the fluctuating flow acting on the TST, caused by the turbulence and wave flow, will contribute to the fatigue of a TST. The importance of incorporating the turbulence effects in turbine simulations to accurately predict both power production and turbine loading has been addressed by previous studies in both site measurements [3, 10, 11] and numerical simulations [12, 13, 14]. Laboratory experiments by Chamorro *et al.* [9] show that in a confined low frequency range, the instantaneous power generated by a turbine can be affected by the ambient turbulent structure. Using the design tool of GH Tidal Bladed [15] strong correlations are found between turbine fatigue loadings and levels of both turbulence intensity and significant wave height. The quantitative investigation of the effects of large-scale turbulence on the instantaneous performance and bending moments of the rotor blades using a large-eddy simulation is provided in [16]. In addition to the combined wave-current coupling feature, the related turbulence metric was investigated in a numerical model by Venugopal *et al.* [17]. Numerical simulations carried out in Tidal Bladed software, using a von Kármán velocity spectra and coherence, indicate that it is important to use appropriate turbulence parameters for the prediction of the structural loading [18]. However, the effects of turbulence structures, of similar dimensions to a turbine rotor diameter, on the blade loadings are not well understood [19]. Additionally, how the smallest dissipation scales of the turbulence will affect the skin-friction drag and flow transition on blades is uncertain [20]. Gaurier *et al.* [21] suggests that analysis at a high turbulence intensity level up to 20% is necessary to understand the nature of the loadings and fatigue of the TST. Generally, a high turbulence intensity is difficult to achieve in an experimental test due to the facility limitations. Therefore, the generation of the full field accounting for co-existing wave and current together with various turbulence intensity levels in a numerical simulation environment is necessary. It will significantly enhance the understanding of the combined effects and benefits the safer design of TSTs.

Recent decades have seen a significant advance in computational technology and the growth in computer hardware capability, and the effort to improve algorithms efficiency and robustness [22, 23, 24, 25]. However, due to its inherent complex structure and Fluid-structure interaction (FSI) feature, the applications of Computational-Fluid Dynamics (CFD) to renewable offshore structures is still computationally costly and unaffordable, and only limited studies have been carried out [5, 12, 26, 27]. The simulation of waves requires a two phase solver and the simulation of scale difference between a potential solver and a turbulent flow solver make the CFD solution even more difficult. Hence, so far, only limited work has considered the wave and turbulence effects [28] and a more affordable tool is desired. To fill the gap, in this study, a novel methodology aimed at modelling the combined effects of tidal currents, gravity waves, and ambient flow turbulence on the dynamic response of a tidal energy converter is proposed. The OpenFAST [29] open-source software package is a multi-physics, multi-fidelity tool for simulating the coupled dynamic response of wind turbines that managed by the National Renewable Energy Lab. It couples computational modules for aerodynamics, hydrodynamics for offshore structures, control and electrical system (servo) dynamics, and structural dynamics to enable coupled nonlinear aero-hydro-servo-elastic simulation in the time domain. Besides, OpenFAST enables the analysis of a range of wind turbine configurations, including two- or three-blade horizontal-axis rotor, pitch or stall regulation, rigid or teetering hub, upwind or downwind rotor, and lattice or tubular tower. As TSTs share similar principles and design method to wind turbines, it is reasonable to take advantage of the OpenFAST code and modify it to apply to TST study. Therefore, OpenFAST is employed to implement the modified algorithm proposed in this research and further investigations are then carried out in order to understand the TST performance when exposed to harsh ocean environments.

In this paper, Section 2 describes the methodology of the wave-current interaction theory. Section 3 demonstrates the generation of the combined wave-current considered in this research. Section 4 is dedicated to the turbulent flow generation. The loading calculation procedure together with the presentation of simulated results, analysis and discussion are further detailed in Section 5. Conclusion of this paper is provided in Section 6.

2. Methodology

2.1. Wave-current interaction theory

In this section, the theory behind the modelling of a linear wave and a uniform current is first introduced. Wave-current models can consider waves travelling on a steady uniform current or waves propagating from an area without current into an area with a steady uniform current [30]. Here only the latter model is discussed and in this case, the wave height, wavelength and wave power transmission are all modified. The fundamental assumptions in the calculation are that: 1) The conditions are steady state - that implies the wave period (or wave frequency), as measured by a stationary observer, is the same before and after the waves run into the changed current. This is generally valid for waves running into a current whose velocity has a positive component in the same direction as the wave is propagating. It is also valid for a wave running into an opposing current, but only if the component of the current resolved against the wave direction is less than the wave celerity. 2) The quantity termed 'Wave Action' is the wave property that is conserved during wave current interaction [31]. This can be interpreted as: in a coordinate system moving with the local current velocity, the energy transmitted by the waves in a wave cycle is a constant. (Note this differs from constant power transfer because, although the wave frequency to a fixed observer is constant, the wave frequency, relative to the current, varies as the current changes.)

To derive the equation for the coupled wave and current, a fixed reference frame with subscript a represents a quantity measured by a stationary observer and a reference frame with subscript r represents a 'relative' quantity measured by an observer moving with the local uniform current velocity U_a are applied. It should be noted that the wave properties of the moving reference frame are same as that of in quiescent water without current situation. Quantities that are the same in both reference frames have neither the a nor r subscript.

The velocity of the wave crest in the fixed frame, the apparent celerity c_a, is represented as the sum of the wave celerity c_r in moving frame and the current velocity U_a:

$$c_a = c_r + U_a \tag{1}$$

Noting,

$$c_a = L/T_a \tag{2}$$

$$c_r = L/T_r \tag{3}$$

and multiplying both left and right-hand side of Equation 1 with the wave number $k = 2\pi/L$ yields the apparent angular frequency ω :

$$\omega_a = \omega_r + kU_a \tag{4}$$

Here ω_r is the relative wave angular frequency in the moving frame and quiescent water wave theory can be applied and ω_r follows the dispersion relation:

$$\omega_r = \sqrt{gktanh\,(kd)} \tag{5}$$

which can be rearranged as:

$$\omega_a - kU_a = \sqrt{gktanh\,(kd)} \tag{6}$$

Here g is the acceleration due to gravity and d is the water depth. Equation 6 can be solved for k by an iteration procedure.

For a steady wave and current, the conservation equation of the wave action [31], given by:

$$\frac{\partial}{\partial x}\left[\frac{E(Cg_r+U_a)}{\omega_r}\right]=0 \tag{7}$$

Here Cg_r is the relative group velocity of the waves and E is the wave energy density. The relationship between the wave energy and wave height (H) can be found as:

$$E=\frac{1}{8}\rho g H^2 \tag{8}$$

In the following, for the wave without current the subscript '0' is used. After the wave propagates into an area with current, the subscript '1' is used. Substituting E into the wave action conservation equation, the wave height H_1 in the current region is:

$$H_1=H_0\sqrt{\frac{\omega_{r1}\,Cg_0}{\omega_a\left(Cg_{r1}+U_a\right)}} \tag{9}$$

In which, the group velocity for the zero-current region (Cg_0) and in current region (Cg_{r1}) can be calculated by, respectively:

$$Cg_0=\frac{1}{2}\frac{\omega_a}{k_0}\left[1+\frac{2k_0d}{sinh\left(2k_0d\right)}\right] \tag{10}$$

$$Cg_{r1}=\frac{1}{2}\frac{\omega_{r1}}{k_1}\left[1+\frac{2k_1d}{sinh\left(2k_1d\right)}\right] \tag{11}$$

For the random wave and current cases, the modified wave spectrum in the presence of the current following the conservation of wave action can be expressed as:

$$S_{\eta 1}\left(\omega_a,U_a\right)=\frac{\omega_{r1}\,Cg_0}{\omega_a\left(Cg_{r1}+U_a\right)}S_{\eta 0}\left(\omega_a\right) \tag{12}$$

The wave spectrum together with the modified complex acceptance H_u and H_a for the horizontal velocity u and horizontal acceleration a give the velocity and acceleration spectra.

$$H_u\left(\omega_{r1}\right)=\omega_{r1}\frac{cosh\left(k_1\left(z+d\right)\right)}{sinh\left(k_1d\right)} \tag{13}$$

$$H_a(\omega_{r1}) = -i\omega_{r1}^2 \frac{cosh(k_1(z+d))}{sinh(k_1 d)} \tag{14}$$

Here ω_r is the relative wave frequency and the relative wave number is solved by the dispersion Equation 6. The horizontal velocity spectrum $S_u(\omega, U)$, thus is given by:

$$S_{u1}(\omega_a, U_a) = |H_u(\omega_{r1})|^2 S_{\eta 1}(\omega_a, U_a) = \omega_{r1}^2 \frac{cosh^2(k_1(z+d))}{sinh^2(k_1 d)} S_{\eta 1}(\omega_a, U_a) \tag{15}$$

and the corresponding acceleration spectra is given by:

$$S_{\dot{u}1}(\omega_a, U_a) = |H_a(\omega_{r1})|^2 S_{\eta 1}(\omega_a, U_a) = \omega_{r1}^2 S_{u1}(\omega_a, U_a) \tag{16}$$

The flow chart (see Figure 1) shows how this procedure was implemented, for the irregular wave, within the OpenFAST algorithm.

2.2. Turbulent flow characteristics and metric

In general, turbulent flow can reach a statistically stationary state if the data time history is collected for a long period of time, i.e. the statistics can be considered independent of time for large sampling period [32]. A velocity component $U(x,t)$ at any time t can be expressed as:

$$U(x,t) = \overline{u} + u'(t) \tag{17}$$

where $\overline{u}$ is the time-averaged mean velocity in the direction of flow and is u' fluctuating component of velocity.

The turbulence metric most commonly used in the tidal energy industries for site turbulence level classification is the turbulence intensity (TI) which can be defined as: [10]

$$TI = \frac{\sigma_u}{\overline{u}} \tag{18}$$

in which, the $\overline{u}$ indicates velocity averaged over a 10-minute duration, σ_u is the standard derivation of fluctuating components u' for a total of Np measurements that can be calculated by:

$$\sigma_u = \sqrt{\frac{\sum_{i=1}^{i=N_p} (u_i')^2}{N_p}} \tag{19}$$

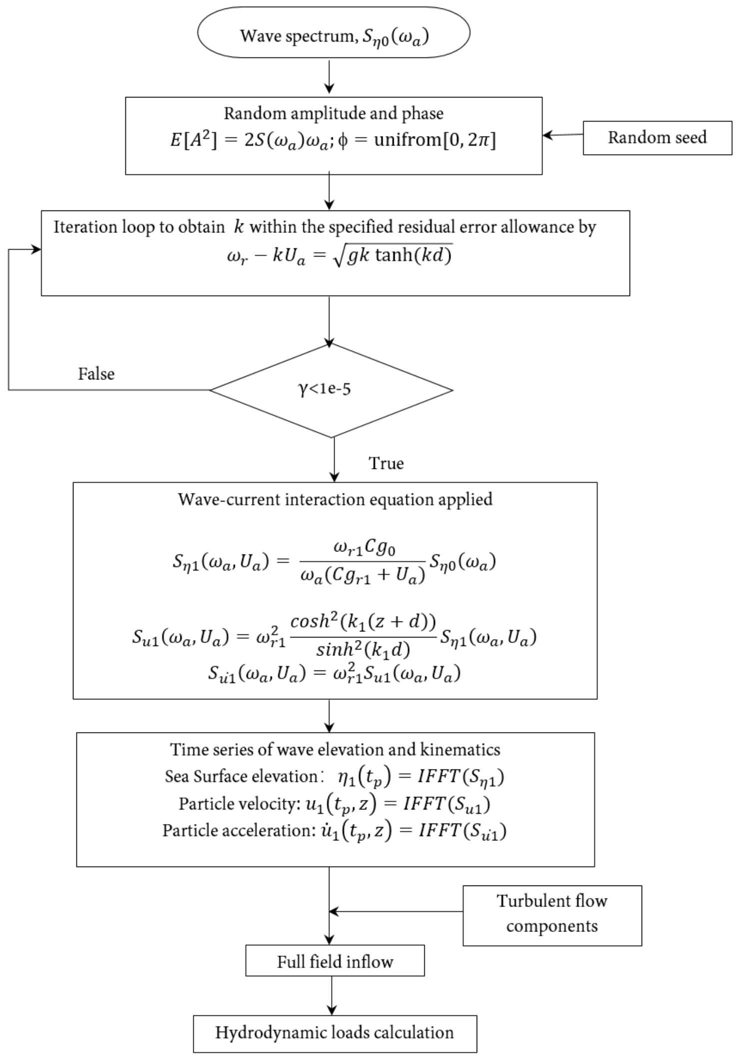

Figure 1: Flow chart of the irregular wave-current coupling procedure

The Reynolds stress for constant density flow can be expressed as $\overline{u_i' u_j'}$. Turbulent kinetic energy (TKE), has also shown a negative impact on power production [33], is defined as one-half the sum of the normal turbulent velocities:

$$TKE = \frac{\overline{u_i' u_i'}}{2} = \frac{1}{2}\left(\overline{u'^2} + \overline{v'^2} + \overline{w'^2}\right) \tag{20}$$

where u', v' and w' are fluctuating components of velocity in three directions.

Coherent turbulent kinetic energy (CTKE), is another metric that closely correlates with the dynamic loads on a turbine, is defined as:

$$CTKE = \frac{1}{2}\left[(u'v')^2 + (u'w')^2 + (v'w')^2\right] \tag{21}$$

3. Combined wave–current generation

Referring to Section 1, the generation of the incident flow with spatial and temporal variation that represents the conditions experienced by a TST is important. In this section, the coupled wave-current flow is generated following Equations 9 and 12 for regular and irregular waves, respectively. To validate the proposed methodology and investigate the mechanism behind the regular/irregular wave and current coupling, the numerical simulations carried out in this section can be split into two categories: (1) by using the original solver (without involving the wave-current coupling) of wave advance on the following/opposing current; (2) by using the modified solver considering the wave-current coupling. The modified solver was validated for regular waves by comparing the results with hand calculations. For irregular waves analysed conditions are chosen to allow comparison with published data.

The regular wave-current interaction theory is first validated with the conditions given in Table 1. For each simulation, a 10-minute long time series is developed with a time step of 0.01s. For the range of current velocity values considered, due to the wave block consideration, the maximum ω in opposing current is predicted as 3.06 which is calculated by $\omega_{max} = -g/(4U_C)$ [34].

Table 1: Regular wave working conditions

Regular wave parameter	Value
Wave height $H(m)$	0.15
Wave period $T_a(s)$	2.5
Current velocity $U_c(m/s)$	+0.8/-0.8
Water depth $d(m)$	2
$\omega_{max}(Hz)$	3.06

From Figure 2 and Figure 3, we can see that water surface elevation and the kinematics can be significantly modified by a current, for instance the differences regarding the wave elevation amplitude are 76% and 97% in the following and opposing current, respectively. Following and opposing

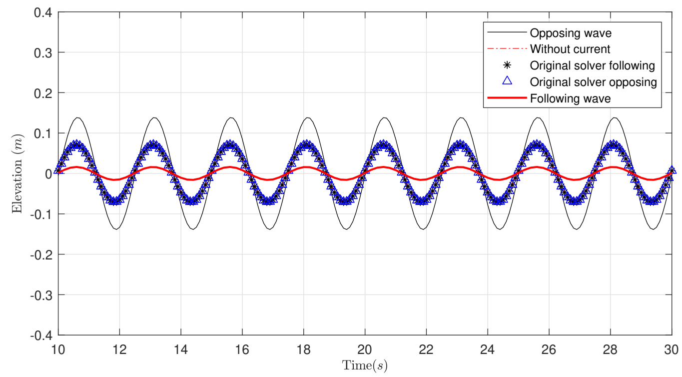

Figure 2: Wave elevation time series simulated using the wave-current interaction theory for the working conditions of (1) following and opposing wave-current using the modified solver, (2) following and opposing wave-current using the original non-coupling solver and (3)wave only without current

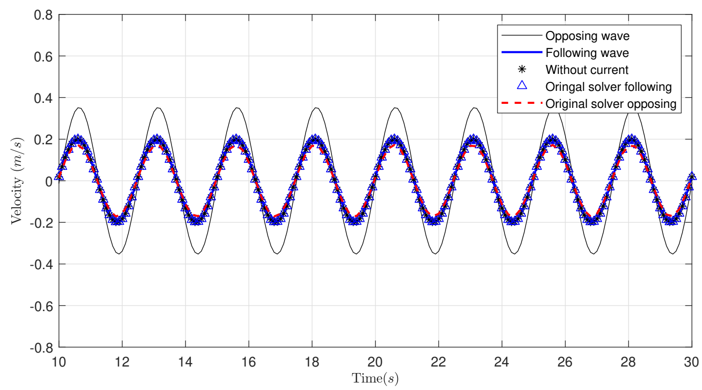

Figure 3: Horizontal wave velocity time series simulated with the wave-current interaction theory for the working conditions of (1) following and opposing wave-current using the modified solver, (2) following and opposing wave-current using the original non-coupling solver and (3)wave only without current

currents show the opposite effect on the wave kinematics. Wave advancing on opposing current results in an increase of the wave elevation and velocity while the following current decreases the magnitude of wave elevation and velocity.

3.1. Tank-scale irregular wave-current test

For the irregular wave generation, a JONSWAP spectrum is applied. A tank scale case is first analysed with the working condition shown in Table

2. The wave elevation and velocity in the time domain for three different working conditions are demonstrated in Figure 4 and 5, which are: (1) wave with following current, (2) wave with opposing current and (3) wave without current.

Table 2: Irregular wave tank scale working conditions

Irregular wave parameter	Value
Significant wave height $H_{m0}(m)$	1.5
Wave period $T_P(s)$	5
Current velocity $U_c(m/s)$	+0.8/-0.8
Water depth $d(m)$	2
Peakness parameter $\gamma(Hz)$	3.3

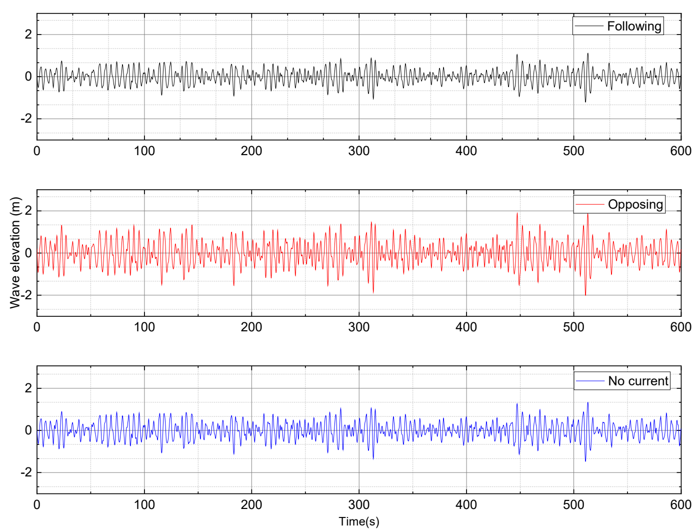

Figure 4: Wave elevation time series for the conditions of (1) wave with following current, (2) wave with opposing current, (3) wave without current

From Figure 4 and 5, as we can see, similar to the regular wave condition, both the wave elevation and velocity have been influenced by the presence of the wave-current interaction. Comparing to the wave only case, the following wave-current condition sees the decrease of the wave elevation and horizontal velocity, whereas the opposite trend is observed in the opposing wave-current condition.

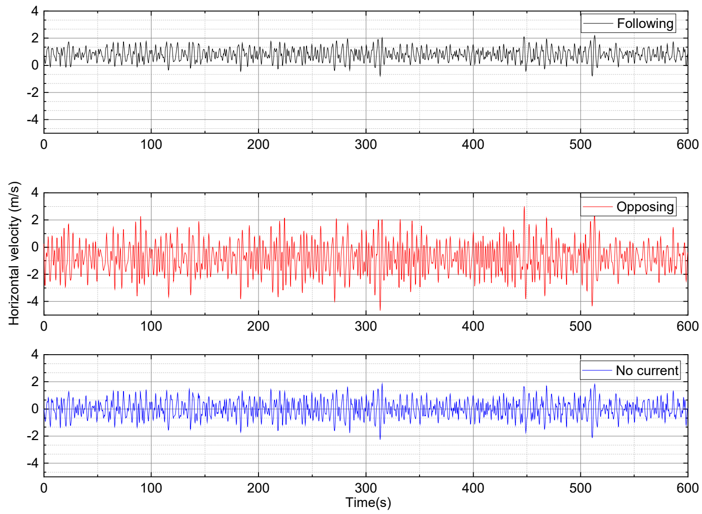

Figure 5: Velocity time series in the horizontal direction for the conditions of (1) wave with following current, (2) wave with opposing current, (3) wave without current.

3.2. Full-scale irregular wave-current test

In this section, the irregular wave theory is examined for a full-scale working condition (see Table 3), in which irregular waves propagate onto a current with a velocity of 3.1 m/s in the water depth of 30 m.

Table 3: Irregular wave full-scale working condition

Significant wave height $H_{m0}(m)$	2.25
Wave period $T_P(s)$	9.68
Current velocity $U_c(m/s)$	3.1
Water depth d(m)	30
Peakness parameter $\gamma(Hz)$	3.3
Hub height $H_u(m)$	15

Figure 6 and Figure 7 show the time series of wave velocity and wave elevation for this full-scale irregular wave-current case, separately. In both figures, the wave velocities involving the wave-current interaction are compared to that of the original solver which do not consider the wave-current interaction. Figure 6 sees the wave velocity increase in the opposing case while decrease in the following case when comparing to the original solver results. In Figure 7, the wave elevations are same in the original following and opposing case since the interaction with current is not involved.

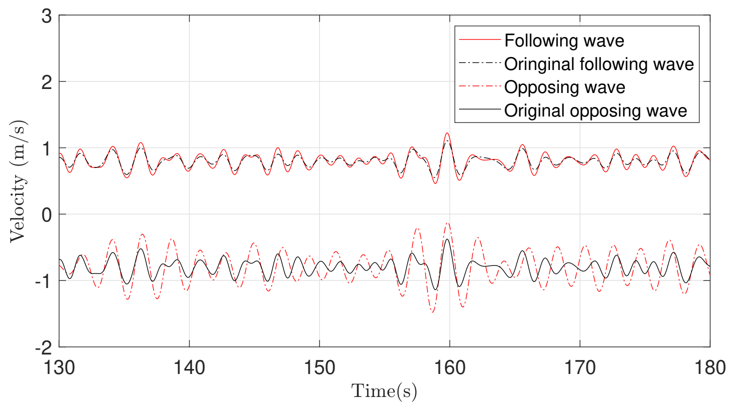

Figure 6: Irregular wave velocity time series for the conditions of (1) wave with following current, (2) wave with opposing current, (3) following wave-current without interaction and (4) opposing wave-current without interaction.

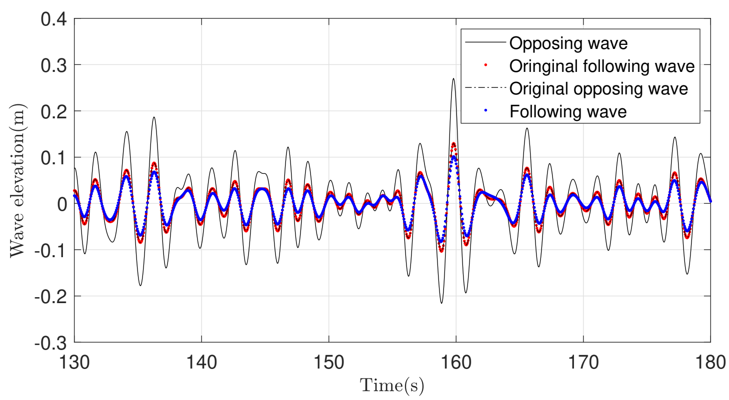

Figure 7: Irregular wave elevation time series for the conditions of (1) wave with following current, (2) wave with opposing current, (3) following wave-current without interaction and (4) opposing wave-current without interaction.

In terms of the frequency domain analysis, the wave elevation spectrum and velocity spectrum are demonstrated in Figure 8 and 9. From these figures, it can be seen that: (1) in the case of an opposing current, waves get steeper due to increase in wave height and shortening of wavelength, which lead to higher spectral densities in the wave elevation spectrum; when the waves and current travel in the same direction, as expected, the wave height decreases but with an increase in wavelength, which results in comparatively lower values of spectral density and (2) the higher velocity gives a higher

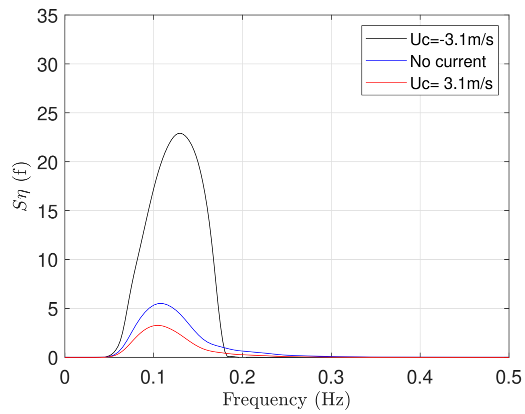

Figure 8: Wave elevation spectra for the conditions of (1) wave with following current, (2) wave with opposing current, (3) wave without current.

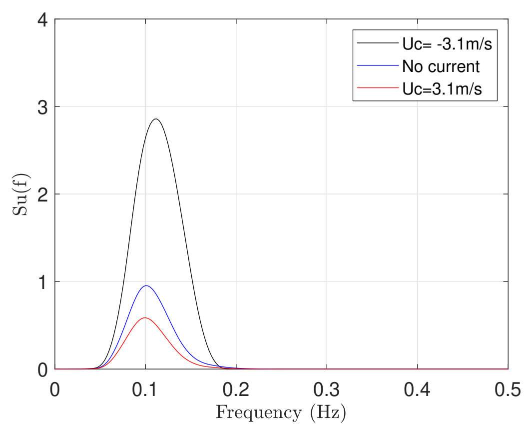

Figure 9: Velocity spectra for the conditions of (1) wave with following current, (2) wave with opposing current, (3) wave without current.

velocity spectrum in the opposing case while lower value in the following case caused by the velocity reduction. More comparisons regarding the significant wave height (H_{m0}) and wave period (T_p) are given in Table 4, in which the significant wave height is calculated by:

$$H_{m0} = 4\sqrt{m_0} \tag{22}$$

where

$$m_0 = \int_0^\infty S_\eta(f) \, f^o df \tag{23}$$

Table 4: Wave kinetic parameters comparison

	Input		Modified Numerical		FloWave test		Difference[%]	
	+	-	+	-	+	-	+	-
$U_c(m/s)$	3.1	-3.1	3.1	-3.1	3.2	-3.2	0	0
$H_{m0}(m)$	2.25	2.25	1.60	5.23	1.56	6.11	2.56	14.4
$T_P(s)$	9.685	9.68	10.15	8.95	9.97	9.18	1.81	2.51

here m_0 is the zeroth moment and $S_\eta(f)$ is the wave energy spectrum.

In Table 4, the results of the proposed numerical method and measurement from FloWave tests are demonstrated with the relative errors between them are given as well. More details of the model test carried out in the FloWave facility can be found in [8]. From Table 4, we can see, the difference between the present numerical method and the test measurement is a maximum of 14.4% for H_{m0} and 2.51% for T_P when subjected to the current in the opposite direction. This indicates that the algorithm applied in this research is reliable and capable of generating a combined wave-current environment with reasonable accuracy.

4. Turbulent flow generation

In addition to the coupled wave and current, the fluctuating component of the velocity in Equation 17 is generated in this section. Within the framework of OpenFAST, the turbulent field is generated by the module of TurbSim [35]. A wide range of turbulence intensities are covered here which are 11.5%, 15.5% and 20%. NREL/UW Tidal Channel spectral model by Levi Kilcher of the National Wind Technology Center is applied for the marine and hydrokinetic (MHK) turbulence [36]. More details of the TIDAL spectral model function can be found in [37]. Following the procedure described in the flow chart in Figure 1, the total velocity time series involving the wave-current and turbulence in u and w-directions can be produced (see Figure 10). The corresponding key turbulence characteristic metric, such as the TKE, CTKE and the turbulent Reynolds stress can be calculated by using the Equation 20 and 21.The time series of these parameters are shown in Figure 11 and 12, receptively.

4.1. The effect of the direction between the wave and current

It is evident that the following and opposing wave directions have different effects on the flow properties. Through the frequency domain analysis

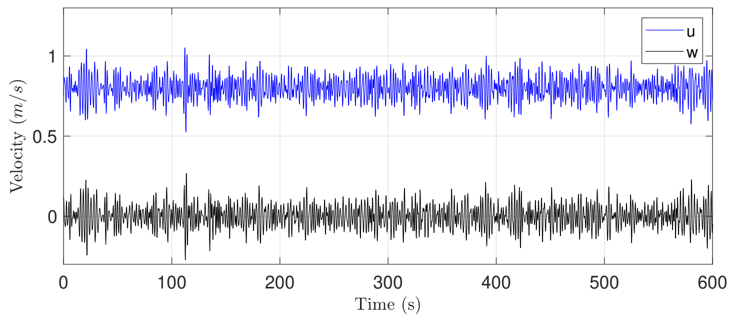

Figure 10: Total velocity considering the wave-current and turbulence

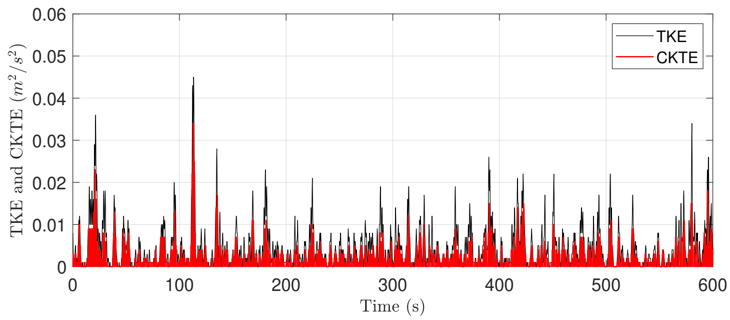

Figure 11: Turbulence kinematic energy and coherence kinematic turbulence energy

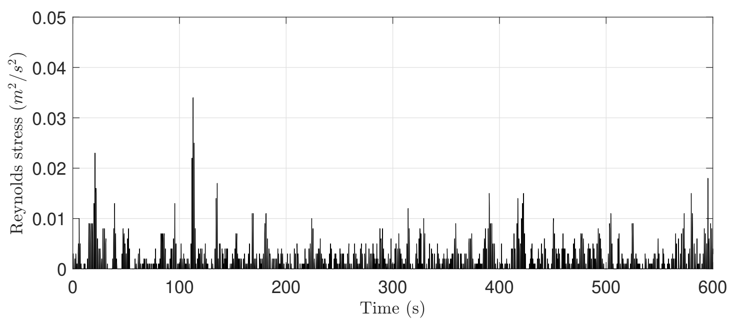

Figure 12: The turbulent Reynolds stress

from Figure 13 to 15, it can be observed that the no-current wave frequency remains the dominant frequency in the following case (see Figure 13) and opposing case (see Figure 14). It should be noted that these velocity spectra are measured at the hub height. The power spectral density (PSD) is larger when the waves oppose the current than in the following condition in Figure 15 (as is well known by Mariners). It is also observed that the waves are only important in a narrow frequency band, again this is expected as waves are usually considered narrow banded whereas turbulence is considered broad banded.

There are dissimilarities in the spectra from one case to another, linked to the wave-current combination and turbulent intensity. In figure 13 and 14, for the current only case, as expected, show higher energy at lower frequencies. The effect of wave is quite obvious where a peak can be found in a low frequency band comparing to the current only case. Particularly, all have their maximum peak centred at around 0.4 Hz. In figure 15, a higher and narrower peak range can be seen in the opposing working condition in comparison to that of the following working conditions.

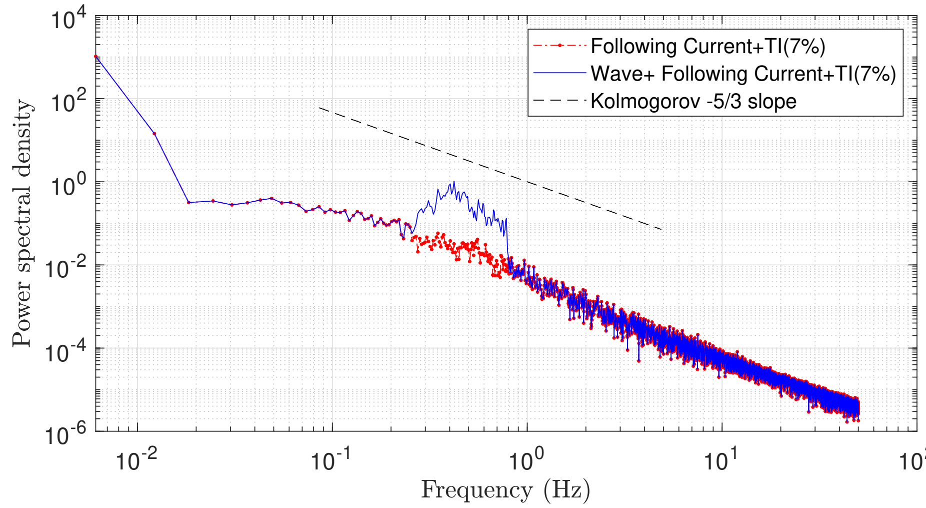

Figure 13: Velocity spectra of (1) following current (Uc=0.8 m/s) with TI=7%; (2) wave advance on the following current (Uc=0.8 m/s) with TI=7%.

4.2. The effect of the turbulence intensity levels

Referring to Section 1, the turbulence intensity level is a significant contributor to the ambient flow around a TST. The effect of different turbulent level can be observed in both the following case (see Figure 16) and opposing case (see Figure 17). Higher TI cases generally result in higher spectral energy across all frequencies, except for the peak frequency range, power are same for different turbulent levels. The peak frequency value for all the three examined intensities are centred around 0.1Hz.

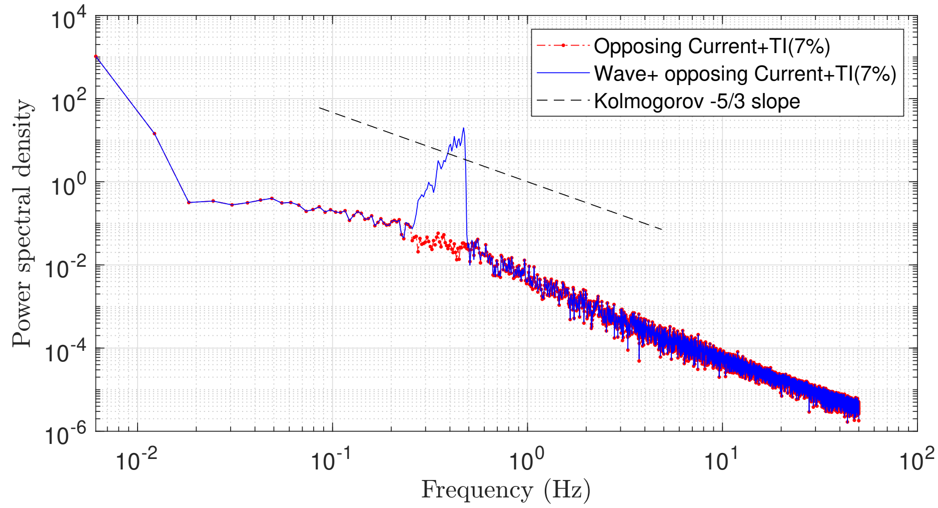

Figure 14: Velocity spectra of (1) opposing current (Uc=-0.8 m/s) with TI=7%; (2) wave advance on the opposing current (Uc=-0.8 m/s) with TI=7%.

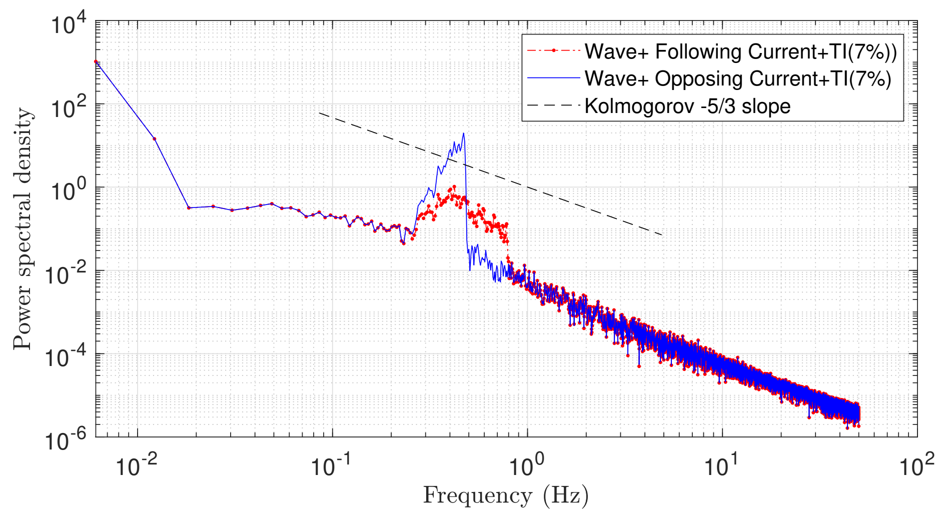

Figure 15: Comparison between the following and opposing velocity spectra of (1) wave with the following current (Uc=0.8 m/s) with TI=7%; (2) wave with the opposing current (Uc=-0.8 m/s) with TI=7%.

5. TST loading simulation

For the numerical simulation here, the 1:15 scale TST with a rotor blade configuration the same as that in the FloWave test [8, 38, 39, 40] is chosen.

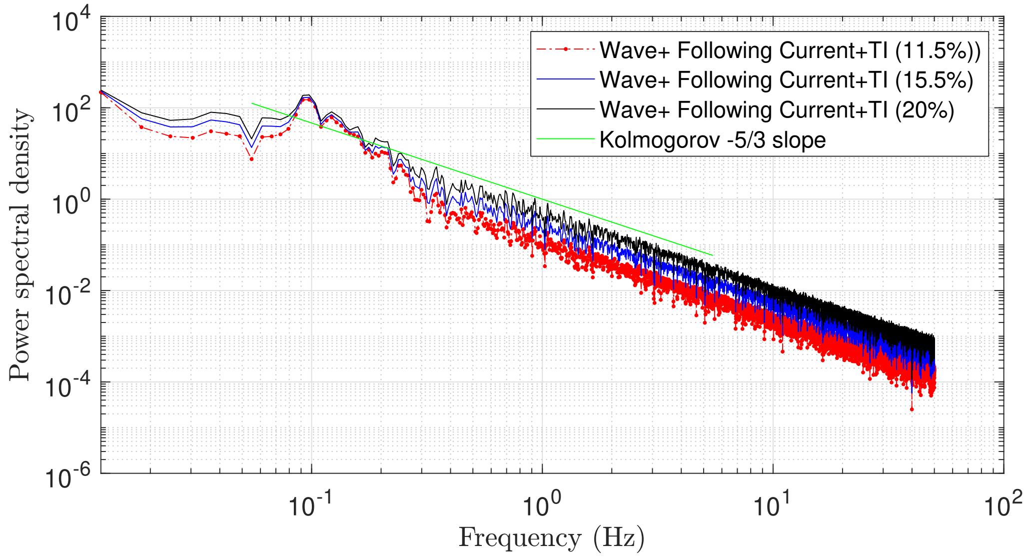

Figure 16: Comparison between the full-scale velocity spectra of different turbulence intensities:(1) 11.5%; (2) 15.5%; (3) 20% for wave with following current.

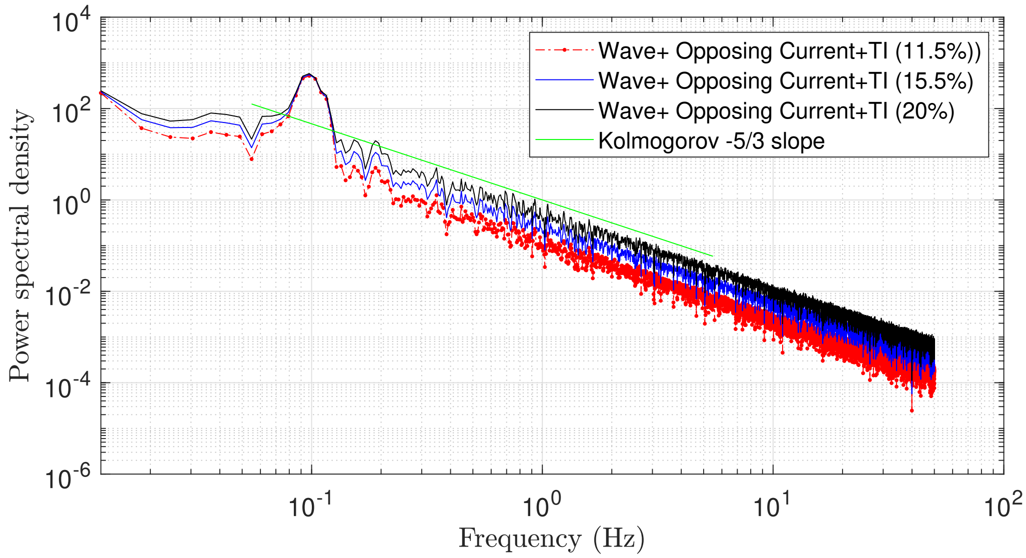

Figure 17: Comparison between the full-scale velocity spectra of different turbulence intensities:(1) 11.5%; (2) 15.5%; (3) 20% for wave with opposing current.

The TST model is a bottom mounted machine with a three-bladed horizontal axis rotor. The rotor radius (D) is 0.6 m and the hub height (H_u) is 1 m [41].

The adopted NACA 63418 blade is characterised by a tip speed ratio (TSR) around 5.75 for the maximum C_p of about 0.45. The details of the turbine are given in Table 5. As with the model test, the generator was operated in speed control mode in the numerical simulations with the rotational velocity, ω_R, set to 90 rpm = 9.42 rad/s. The simulations were carried out at a nominal flow speed of 0.8 m/s which results in a corresponding TSR value of 7.

Table 5: Turbine specifications

Number of blades	3
Rotor Radius (m)	0.6
Nacelle length (m)	1.03
Nacelle diameter (m)	0.12 from hub
Hub height (m)	1
TSR	2-7

Figure 18 shows three key parameters: stream-wise root bending moment (RBM), thrust (T) and power (P) under the following and opposing wave scenarios. Here a turbulence intensity (TI) equal to 7% is modelled since the FloWave test turbulence intensity is approximately 7% for this flow velocity. It is clear that the fluctuation amplitude of all parameters experiences a significant rise in the opposing wave condition. However, the effect for the following wave is limited, where the mean value remains the same. Additionally, the same wave-current working conditions with higher turbulence intensity TI=20% is presented in Figure 19. The key parameters predicted are similar to the TI=7% case in that a big increase in the opposing wave condition is demonstrated. More insights can be gained from Table 6 to Table 10 which show the statistics of the key parameters. The outputs of the proposed numerical method in irregular waves are compared to that measured in the FloWave test [8] (see Table 8). The numerical results are close to measured data in both following and opposing wave conditions based on the mean values of the three examined parameters. The maximum absolute difference is 16% for the RBM in the opposing wave case. However, there are larger differences between the standard derivations. The maximum difference (around 44%) occurs for the opposing case as well as for the thrust T. The discrepancy may be caused by the difference in the turbulent flow distribution between the experimental model test and configuration in the

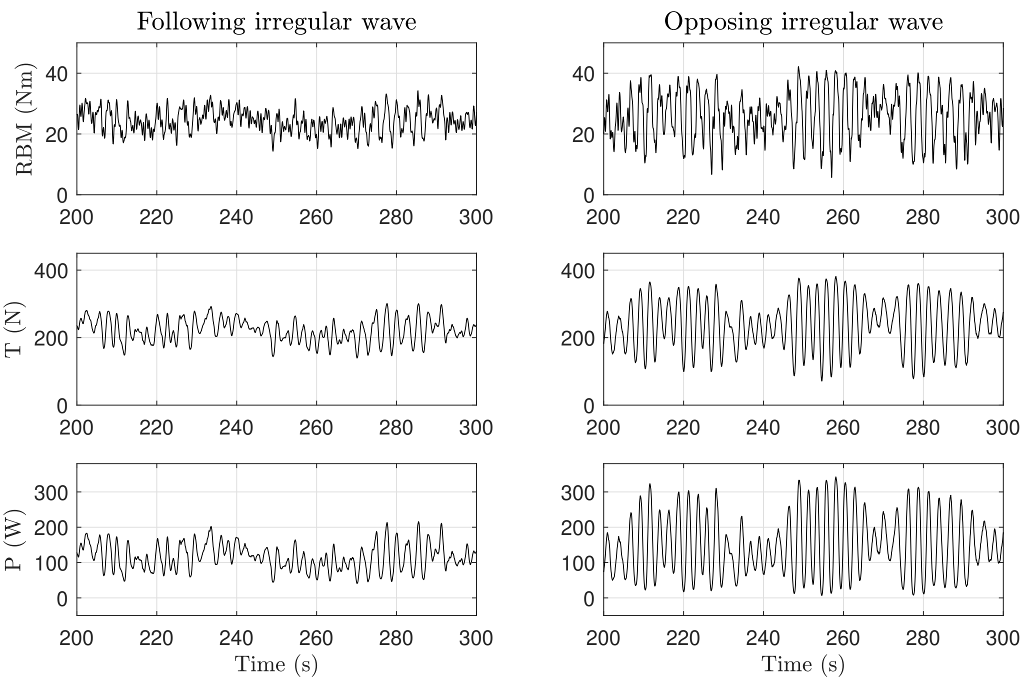

Figure 18: Time history of the key turbine parameters for the opposing and following wave conditions with the turbulence intensity TI=7%.

numerical simulation.

From Tables 6 to 10, the results predicted by the non-coupled original solver are significantly different to that of the modified solver. This affects all the working conditions output, most notably the standard derivations of the parameters. In particular, comparing the properly coupled calculation with a more approximate uncoupled calculation, the opposing wave cases result in a much larger difference than the following wave case. For instant, for the TI=20% case, overestimated values are provided by the original solver for all the three parameters of the following wave case, and the corresponding absolute differences are 9.5%, 9.2% and 8.8%, for the RBM, T and P, respectively. However, underestimated values are given by the original solver for the opposing case with the much larger absolute differences of 40.3%, 39.2% and 36.2%, respectively. Referring the section 2 and 3 and the quantitative data in these tables (Table 6 and 9 for regular wave and Table 7 and 10 for irregular wave) both the regular and irregular waves are subjected to the effect caused by the wave-current interaction, and followed the same trend.

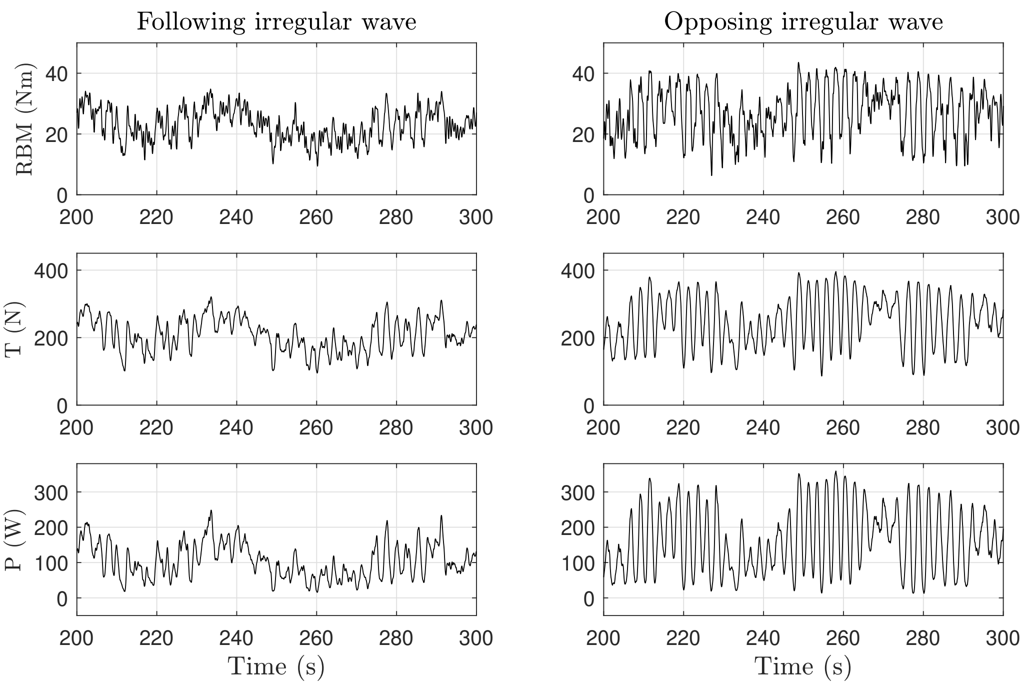

Figure 19: Time history of the key turbine parameters for the opposing and following wave conditions with the turbulence intensity TI=20%.

Regarding the turbulence level dependence, more understanding is obtained by comparing the outputs between the low (7%), high disturbance (20%) and no turbulence cases. Firstly, from the comparison between the no turbulence and original solver solution in Table 6, all the standard derivation values are underestimated if the ambient turbulent effect is excluded, particularly for the opposing case. Secondly, further increase of the turbulence level contributes to the change of loading amplitude, for example, the outputs from the following wave case with TI=20% are found to exceed the TI=7% values by 36.5%, 44.6% and 45.6% for the RBM, T and P, respectively.

The results presented and discussed above ideally need additional simulations and validations to prove the proposed method. Access to data from a real tidal turbine along with spatial current and wave data would also be very beneficial. Hence the actual result values presented here should be treated with caution. In future work, as the coupled wave-current-turbulence interaction is expected to affect the fatigue damage of TST components, fatigue assessment is necessary. Using the proposed methodology, more understand-

Table 6: Standard deviations and means of various environmental and turbine parameters for regular waves TI=7%

Working condition	RBM (Nm)		T (N)		P (W)	
	μ	σ	μ	σ	μ	σ
Without turbulence	25.4	4.6	232.0	36.7	128.9	42.4
Following wave no interaction	25.4	5.0	231.7	41.3	129.6	47.5
Opposing wave no interaction	25.2	6.7	230.2	60.2	133.4	67.8
Coupled following wave	25.5	4.1	232.8	33.5	128.4	38.4
Coupled opposing wave	24.2	8.5	228.1	88.8	141.2	90.6

Table 7: Standard deviations and means of various environmental and turbine parameters for irregular waves TI=7%

Working condition	RBM (Nm)		T (N)		P (W)	
	μ	σ	μ	σ	μ	σ
Following wave no interaction	25.5	4.7	232.7	40.2	129.5	45.4
Opposing wave no interaction	25.4	4.9	232.5	42.3	129.8	48.5
Coupled following wave	28.5	3.9	233.3	33.0	128.4	37.2
Coupled opposing wave	25.1	7.9	228.6	69.8	135.4	77.8

Table 8: FloWave test measurement of standard deviations and means of various environmental and turbine parameters for irregular waves TI=7%

Working condition	RBM (Nm)		T (N)		P (W)	
	μ	σ	μ	σ	μ	σ
Coupled following wave	29.5	3.6	261	28	122	26
Coupled opposing wave	29.1	8.7	256	39	124	65

ing of TST fatigue in the complex wave and turbulent current environment can be gained.

6. Conclusion

In this research, the environmental inflow conditions resulting from the combined action of waves-currents-turbulence are generated by modifications made to the algorithm in the OpenFAST software suite, which accounts for the wave-current interactions. The modifications are targeted at evaluating the performance of a three-bladed horizontal axis tidal stream energy converter subjected to wave-current interaction. The nonlinear physics observed suggests that the flow properties are significantly altered by wave-current-turbulence interactions, which indicates the importance of including the wave-current-turbulence interactions in the tidal turbine modelling. The

Table 9: Standard deviations and means of various environmental and turbine parameters for regular waves TI=20%

Working condition	RBM (Nm)		T (N)		P (W)	
	μ	σ	μ	σ	μ	σ
Following wave no interaction	25.3	6.2	230.5	53.8	131.7	60.9
Opposing wave no interaction	25.1	7.6	229.1	68.6	135.3	76.2
Coupled following wave	25.4	5.5	231.5	48.4	130.6	55.2
Coupled opposing wave	24.1	13.6	218.0	126.1	152.3	128.8

Table 10: Standard deviations and means of various environmental and turbine parameters for irregular waves TI=20%

Working condition	RBM (Nm)		T (N)		P (W)	
	μ	σ	μ	σ	μ	σ
Following wave no interaction	23.4	5.9	231.5	52.6	131.8	59.9
Opposing wave no interaction	25.3	6.1	231.2	54.3	131.8	61.6
Coupled following wave	25.4	5.4	232.1	47.8	130.5	54.2
Coupled opposing wave	24.9	8.5	227.3	75.6	136.2	83.9

wave kinematics determined from the modified solution accounting for wave-current-turbulence interaction are used in the prediction of the hydrodynamic loads on the TST and power generation in a wide range of regular and irregular wave-current conditions, of varying turbulence intensities, both in the following and opposing wave directions to the current. It was founded that the wave-current interactions play a significant role on the loadings and turbine's power performance prediction, especially under the opposing wave-current condition with a difference of about 40.3%; this implies that the coupling effects should not be ignored in the TST modelling. Besides, the turbulence intensity is a key contributor to the TST loading, as the difference between the turbine's responses in different turbulence intensity levels (TI=7% and TI=20%) can be as large as 45.6%. Additionally, the quantitative loading outputs in irregular waves are compared to the data measured in the FloWave experiments. The validation result indicates that the OpenFAST software together with the modified algorithm is capable of wave-current-turbulence flow generating and turbine performance assessment, and can be applied to other working conditions.

7. CRediT authorship contribution statement

Qian Li: Conceptualization, Methodology, Software, Validation, Formal analysis, Writing-original draft preparation. Vengatesan Venugopal: Conceptualization, Methodology, Writing-review and editing, Supervision, Project administration, Funding acquisition. Nigel Barltrop: Conceptualization, Methodology, Writing-review and editing, Supervision, Project administration, Funding acquisition.

8. Acknowledgments

The authors are grateful for financial support from the UK Engineering and Physical Sciences Research Council through FloWTurb (EP/N021487/1). The authors are extremely grateful to the contributions received from industrial partners and research staff of FloWTurb project team.

9. Declaration of Competing Interest

The authors declare that they have no known competing financial interests or personal relationships that could have appeared to influence the work reported in this paper.

Nomenclature

η Water surface elevation $[m]$

γ Peakness parameter $[Hz]$

μ Means value

ν Kinematic viscosity $[m^2/s]$

ω Angular frequency $[rad/s]$

ω_a Wave angular frequency $[rad/s]$

ω_R Rotational velocity $[rmp]$

ω_r Relative wave angular frequency $[rad/s]$

ω_{max} Maximum omega in opposing current $[rad/s]$

ω_{r1} Wave angular frequency noted by an observer moving with the current $[rad/s]$

$\overline{u}$ Time-averaged mean velocity $[m/s]$

$\overline{u_i'u_j'}$ Reynolds stress $[m^2/s^2]$

ρ Water density $[kg/m^3]$

σ_u Standard deviations of the velocity

σ Standard deviation

c_a Apparent celerity $[m/s]$

c_r Wave celerity $[m/s]$

C_{g0} Relative wave group velocity $[m/s]$

C_{gr} Relative group velocity $[m/s]$

$CTKE$ Coherence kinematic turbulence energy $[m^2/s^2]$

d Water depth $[m]$

E Wave energy density $[J/m^2]$

f_p Peak frequency $[Hz]$

g Gravity acceleration $[m/s^2]$

H Wave height $[m]$

H_0 Wave height at zero-current region $[m]$

H_1 Wave height at current region $[m]$

H_u Hub height $[m]$

H_{m0} Significant wave height $[m]$

k Wave number

k_0 Wave number at non-current region

k_1 Wave number at current region

L Wave length $[m]$

m_0 The zeroth moment

N_P Measurement sample numbers

P Power $[W]$

R Rotor radius $[m]$

RBM Stream-wise root bending moment $[Nm]$

$S(\omega)$ Power spectral density $[m^2/rad/Hz]$

$S_\eta(f)$ Wave energy spectrum $[m^2/Hz]$

$S_u(\omega_a, U_a)$ Horizontal velocity spectrum in the current region $[m^2/rad/Hz]$

$S_{\dot{u}}(\omega_a, U_a)$ Spectral density of horizontal water-particle acceleration in the current region $[m^2/rad/Hz]$

$S_{\eta 0}(\omega_a)$ Spectral density of surface elevation at zero-current region $[m^2/rad/Hz]$

$S_{\eta 1}(\omega_a, U_a)$ Spectral density of surface elevation at current region $[m^2/rad/Hz]$

T Rotor thrust $[N]$

T_a Wave period noted by a stationary observer $[s]$

T_p Significant wave period $[s]$

T_r Relative wave period)$[s]$

TI Turbulence intensity [%]

TKE Turbulence kinematic energy $[m^2/s^2]$

$u(t)$ Instantaneous axial velocity $[m/s]$

U_a Uniform current velocity $[m/s]$

U_c Current velocity $[m/s]$

$u'(t)$ Fluctuation of x-direction velocity $[m/s]$

$v'(t)$ Fluctuation of y-direction velocity $[m/s]$

$w'(t)$ Fluctuation of z-direction velocity $[m/s]$

References

[1] E. M. E. LTD, Tidal developers, 2010. URL: http://www.emec.org.uk/marine-energy/tidal- developers/.

[2] S. Draycott, J. Steynor, T. Davey, D. M. Ingram, Isolating incident and reflected wave spectra in the presence of current, Coastal Engineering Journal 60 (2018) 39–50. URL: https://doi.org/10.1080/05785634.2017.1418798. doi:10.1080/05785634.2017.1418798.

[3] B. G. Sellar, D. R. Sutherland, D. M. Ingram, V. Venugopal, Measuring waves and currents at the European marine energy centre tidal energy test site: Campaign specification, measurement methodologies and data exploitation, OCEANS 2017 - Aberdeen 2017-Octob (2017) 1–7. doi:10.1109/OCEANSE.2017.8085001.

[4] S. Draycott, D. Noble, T. Davey, J. Steynor, D. M. Ingram, Application of Complex Wave and Current Conditions in a Laboratory Environment, EWTEC Conference Proceedings (2017) 1–8.

[5] S. C. Tatum, C. H. Frost, M. Allmark, D. M. O'Doherty, A. Mason-Jones, P. W. Prickett, R. I. Grosvenor, C. B. Byrne, T. O'Doherty, Wave-current interaction effects on tidal stream turbine performance and loading characteristics, International Journal of Marine Energy 14 (2016) 161–179. URL: `http://dx.doi.org/10.1016/j.ijome.2015.09.002`. doi:10.1016/j.ijome.2015.09.002.

[6] S. Draycott, J. Steynor, A. Nambiar, B. Sellar, V. Venugopal, Experimental assessment of tidal turbine loading from irregular waves over a tidal cycle, Journal of Ocean Engineering and Marine Energy 5 (2019) 173–187.

[7] T. de Jesus Henriques, S. Tedds, A. Botsari, G. Najafian, T. Hedges, C. Sutcliffe, I. Owen, R. Poole, The effects of wave-current interaction on the performance of a model horizontal axis tidal turbine, International Journal of Marine Energy 8 (2014) 17–35.

[8] S. Draycott, J. Steynor, A. Nambiar, B. Sellar, V. Venugopal, Experimental assessment of tidal turbine loading from irregular waves over a tidal cycle, Journal of Ocean Engineering and Marine Energy 5 (2019) 173–187. doi:10.1007/s40722-019-00136-9.

[9] L. P. Chamorro, C. Hill, S. Morton, C. Ellis, R. E. Arndt, F. Sotiropoulos, On the interaction between a turbulent open channel flow and an axial-flow turbine, Journal of Fluid Mechanics 716 (2013) 658–670. doi:10.1017/jfm.2012.571.

[10] B. G. Sellar, G. Wakelam, D. R. Sutherland, D. M. Ingram, V. Venugopal, Characterisation of tidal flows at the european marine energy centre in the absence of ocean waves, Energies 11 (2018) 1–23. doi:10.3390/en11010176.

[11] M. Dorward, B. Sellar, C. Old, P. R. Thies, Currents, Waves and Turbulence Measurement: A View from Multiple Industrial-Academic Projects in Tidal Stream Energy, 2019 IEEE/OES 12th

Current, Waves and Turbulence Measurement, CWTM 2019 (2019). doi:10.1109/CWTM43797.2019.8955294.

[12] A. Rahman, V. Venugopal, J. Thiebot, On the accuracy of three-dimensional actuator disc approach in modelling a large-scale tidal turbine in a simple channel, Energies 11 (2018). doi:10.3390/en11082151.

[13] V. Venugopal, R. Nemalidinne, Omae2014-24027 Marine Energy Resource Assessment for Orkney and Pentland, Proceedings of the ASME 2014 33rd International Conference on Ocean, Offshore and Arctic Engineering (2014) 1–9.

[14] V. Venugopal, R. Nemalidinne, Marine energy resource assessment for orkney and pentland waters with a coupled wave and tidal flow model, in: International Conference on Offshore Mechanics and Arctic Engineering, volume 45547, American Society of Mechanical Engineers, 2014, p. V09BT09A010.

[15] G. N. Mccann, Tidal current turbine fatigue loading sensitivity to waves and turbulence a parametric study, Methodology (2007).

[16] P. Ouro, T. Stoesser, Impact of Environmental Turbulence on the Performance and Loadings of a Tidal Stream Turbine, Flow, Turbulence and Combustion 102 (2019) 613–639. doi:10.1007/s10494-018-9975-6.

[17] V. Venugopal, A. Vögler, B. Sellar, et al., Characterisation of wave-tidal current-turbulence interactions at tidal energy sites in the orkney islands, in: The 28th International Ocean and Polar Engineering Conference, International Society of Offshore and Polar Engineers, 2018, pp. 813–821.

[18] S. G. Parkinson, W. J. Collier, Model validation of hydrodynamic loads and performance of a full-scale tidal turbine using tidal bladed, International Journal of Marine Energy 16 (2016) 279–297.

[19] B. G. Sellar, D. R. Sutherland, Tidal Energy Site Characterisation At the Fall of Warness , Emec , Uk Energy Technologies Institute Redapt Ma1001 (Md3.8), Technical Report December, The University of Edinburgh, 2016. URL: `http://redapt.eng.ed.ac.uk`.

[20] H. Homann, J. Bec, R. Grauer, Effect of turbulent fluctuations on the drag and lift forces on a towed sphere and its boundary layer, arXiv preprint arXiv:1012.5205 (2010).

[21] B. Gaurier, P. Davies, A. Deuff, G. Germain, Flume tank characterization of marine current turbine blade behaviour under current and wave loading, Renewable Energy 59 (2013) 1–12.

[22] Q. Li, J. Wang, S. Yan, J. Gong, Q. Ma, A zonal hybrid approach coupling FNPT with OpenFOAM for modelling wave-structure interactions with action of current, Ocean Systems Engineering 8 (2018) 381–407. doi:10.12989/ose.2018.8.4.381.

[23] Q. Li, A hybrid model based on functional decomposition for vortex shedding simulations, Ph.D. thesis, City, University of London, 2017. doi:10.1111/etap.12031.

[24] D. O. Edmund, A Velocity Decomposition Method for Efficient Numerical Computation of Steady External Flows., Ph.D. thesis, The University of Michigan, 2012.

[25] P. R. Spalart, Strategies for turbulence modelling and simulations, International journal of heat and fluid flow 21 (2000) 252–263.

[26] M. G. Gebreslassie, G. Tabor, M. R. Belmont, Cfd simulations for sensitivity analysis of different parameters to the wake characteristics of tidal turbine, Open Journal of Fluid Dynamics (2012).

[27] A. Rahman, V. Venugopal, J. Thiebot, On the accuracy of three-dimensional actuator disc approach in modelling a large-scale tidal turbine in a simple channel, Energies 11 (2018) 2151.

[28] U. Ahmed, D. Apsley, I. Afgan, T. Stallard, P. Stansby, Fluctuating loads on a tidal turbine due to velocity shear and turbulence: Comparison of cfd with field data, Renewable Energy 112 (2017) 235–246.

[29] B. J. Jonkman, J. M. Jonkman, FAST v8.16.00a-bjj User's Guide 2016, National Renewable Energy Laboratory (2016) 58.

[30] T. Hedges, Combinations of waves and currents: an introduction, Proceedings of the Institution of Civil Engineers 82 (1987) 567–585.

[31] I. G. Jonsson, Wave-current interactions, The Sea: Ocean Engineering Science 9 (1990) 65–119.

[32] S. B. Pope, Turbulent flows, 2001.

[33] S. Wharton, J. K. Lundquist, Atmospheric stability affects wind turbine power collection, Environmental Research Letters 7 (2012) 014005.

[34] R. M. Moreira, D. H. Peregrine, Nonlinear interactions between deep-water waves and currents, Journal of Fluid Mechanics 691 (2012) 1–25. doi:10.1017/jfm.2011.436.

[35] B. J. Jonkman, J. Buhl, M. L., TurbSim User's Guide, Technical Report September, NREL, 2006. URL: `http://www.osti.gov/servlets/purl/891594-Un9gSK/`. doi:10.2172/891594.

[36] N. Kelley, B. Jonkman, Overview of the TurbSim stochastic inflow turbulence simulator: Version 1.21 (revised february 1, 2001), Technical Report, National Renewable Energy Lab.(NREL), Golden, CO (United States), 2007.

[37] B. J. Jonkman, TurbSim user's guide: Version 1.50, Technical Report, National Renewable Energy Lab.(NREL), Golden, CO (United States), 2009.

[38] G. S. Payne, T. Stallard, R. Martinez, Design and manufacture of a bed supported tidal turbine model for blade and shaft load measurement in turbulent flow and waves, Renewable Energy 107 (2017) 312–326. doi:10.1016/j.renene.2017.01.068.

[39] G. S. Payne, T. Stallard, R. Martinez, T. Bruce, Variation of loads on a three-bladed horizontal axis tidal turbine with frequency and blade position, Journal of Fluids and Structures 83 (2018) 156–170.

[40] R. Martinez, G. S. Payne, T. Bruce, The effects of oblique waves and currents on the loadings and performance of tidal turbines, Ocean Engineering 164 (2018) 55–64.

[41] G. S. Payne, T. Stallard, R. Martinez, Design and manufacture of a bed supported tidal turbine model for blade and shaft load measurement in turbulent flow and waves, Renewable Energy 107 (2017) 312–326.